DOI: 10.1002/chem.200800304

Intrachain Electron and Energy Transfer in Conjugated Organometallic Oligomers and Polymers

Shawkat Mohammed Aly,[a, b] Cheuk-Lam Ho,[c] Daniel Fortin,[a] Wai-Yeung Wong,*[c] Alaa S. Abd-El-Aziz,[b] and Pierre D. Harvey*[a]

Abstract: The synthesis of polymers of the type (-**Cz**-C≡C-PtL_2-C≡C-**Cz**-**X**-)$_n$ along with the corresponding model compounds (Ph-PtL'_2-C≡C-**Cz**)$_2$-**X**-, where **Cz** = 3,3′-carbazole, **X** = nothing, **Cz**, or **F** (2,2′-fluorene), L = PBu_3, and L′ = PEt_3 are reported. The electronic spectra (absorption, excitation, emission, and ns-transient spectra) and the photophysics of these species in 2-methyltetrahyrofuran (2MeTHF) at 298 and 77 K are presented. Evidence for singlet electron and triplet energy transfer from the **Cz** chromophore to the **F** moiety are provided and discussed in detail. The rate for electron transfer is very fast ($>4\times10^{11}\,s^{-1}$), whereas that for triplet–triplet energy transfer is much slower ($\approx10^{3}\,s^{-1}$). This work represents a very rare example of studies that address electronic communication in the backbone of a conjugated organometallic polymer.

Keywords: alkynes · electron transfer · energy transfer · fluorene · metallopolymers · phosphorescence · platinum

Introduction

While mixed-aryl carbazole–fluorene-containing organic dyads, polyads, oligomers, polymers- and dendrimers[1–5] have been the subject of intense research in relation to photo- and electro-luminescence with potential applications in photonics such as photovoltaic cells and organic (OLED) and polymer light-emitting diodes (PLED), the corresponding organometallic polymers have been relatively much less investigated so far from a photophysical point of view.[6–8] These carbazole (**Cz**) and fluorene (**F**) moieties are prone to singlet electron transfer[9,10] and triplet–triplet energy transfer,[9,10] including the case in the **Cz**–**F** dyad,[11] and hence bear important properties that have implications in photonics. Recently, heavy-metal bis(ethynyl) linkers were used to form conjugated carbazole- and fluorene-based bis(ethynyl)–metal polymers (metal = platinum, gold, and mercury), and their emission spectroscopy and photophysics were investigated.[6] The key feature is that incorporation of a heavy metal in the backbone of the polymers can enhance intersystem crossing, hence leading to an increase in the population of the triplet states. This, in turn, leads on the one hand to the potential application of white light emission, a current topic of intense research in OLEDs and PLEDs, but also from a fundamental point of view, to other channels of photo-induced electronic communication across the backbone such as triplet–triplet energy transfer. To our knowledge, no detailed investigation of (donor–acceptor)-containing organometallic polymers exists to date.

Herein we report the synthesis of polymers of the type (-**Cz**-C≡C-PtL_2-C≡C-**Cz**-**X**-)$_n$ along with the corresponding model compounds (Ph-PtL'_2-C≡C-**Cz**)$_2$-**X**-, in which **Cz** = 3,3′-carbazole, **X** = nothing, **Cz**, or **F** (2,2′-fluorene), L = PBu_3, and L′ = PEt_3 (see the structures in Scheme 1). The electronic spectra and the photophysics of these species in 2-methyltetrahydrofuran (2MeTHF) at 298 and 77 K are presented. A discussion of the evidence for singlet and triplet energy transfer from the **Cz** chromophore to the **F** moiety is made. The rate for electron transfer is fast ($>4\times10^{11}\,s^{-1}$), whereas that for triplet–triplet energy transfer is much slower ($\approx10^{3}\,s^{-1}$). This work represents a very rare example of detailed investigations that address electronic

[a] S. M. Aly, D. Fortin, Prof. P. D. Harvey
Département de chimie, Université de Sherbrooke
2550 Boul. Université, Sherbrooke, PQ, J1K 2R1 (Canada)
E-mail: Pierre.Harvey@USherbrooke.ca

[b] S. M. Aly, Prof. A. S. Abd-El-Aziz
Department of Chemistry, University of British Columbia
Okanagan, 3333 University Way, Kelowna, BC, V1V 1V7 (Canada)

[c] Dr. C.-L. Ho, Prof. W.-Y. Wong
Department of Chemistry and Centre for Advanced Luminescence Materials
Hong Kong Baptist University, Waterloo Road, Hong Kong (China)
E-mail: rwywong@hkbu.edu.hk

Supporting information for this article is available on the WWW under http://dx.doi.org/10.1002/chem.200800304.

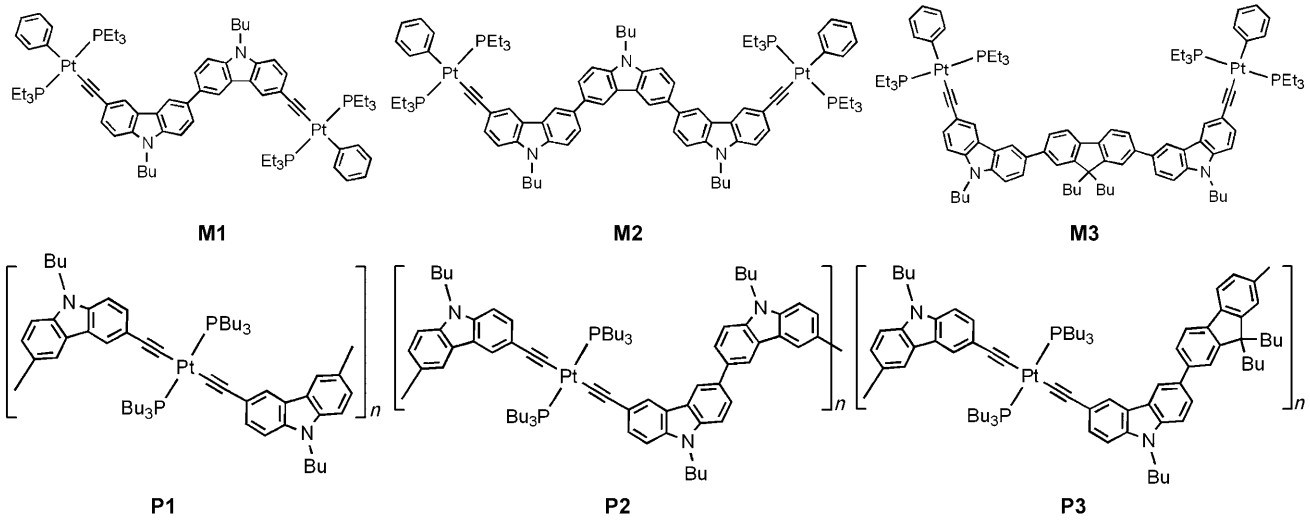

Scheme 1. Structures of organometallic polyynes and their model complexes.

communication in the backbone of a conjugated organometallic polymer.

Results and Discussion

Synthesis and characterization

The precursors **Ia**–**IIIa** were synthesized by a Suzuki palladium-catalyzed cross-coupling reaction between carbazole 3-boronic acid[11d] and a formal electrophile (i.e. **Cz**-Br, Br-**Cz**-Br, or Br-**F**-Br). When these carbazole and carbazole–fluorene oligomeric chromophores were subjected to bromination, a series of new dibromide precursors was prepared. The diethynyl compounds **L1**–**L3** were prepared by applying a palladium-catalyzed Sonogashira coupling reaction sequence. These were then converted to the diethynyl organic precursors in moderate yields following a proto-desilylation by using K_2CO_3 in MeOH as the base (Scheme 2).

Scheme 3 shows the chemical structures and the synthesis of the Pt^{II} metallopolymers **P1**–**P3** and their model dinuclear complexes **M1**–**M3** in the present investigation. The desired Pt^{II} diynes were isolated by preparative TLC plates on silica. For **P1**–**P3**, purification was achieved by filtering the crude sample through a short column using pure CH_2Cl_2 as the eluent. High purity products can be obtained by precipitating the polymer solution in CH_2Cl_2 from MeOH.

All of the new metal complexes and polymers are air-stable and generally exhibit good solubility in chlorocarbons such as CH_2Cl_2 and $CHCl_3$. GPC analysis was used to estimate the molecular weight of each polymer (see data in the Experimental Section). However, the data should be viewed with caution in view of the difficulties associated with utilizing GPC for rigid-rod polymers, which have appreciable differences in the hydrodynamic behavior from those for flexible polystyrene polymers. Hence, we would anticipate certain systematic errors in the GPC measurements. However, the lack of discernible resonances that could be attributed to end groups in the NMR spectra provides support for the

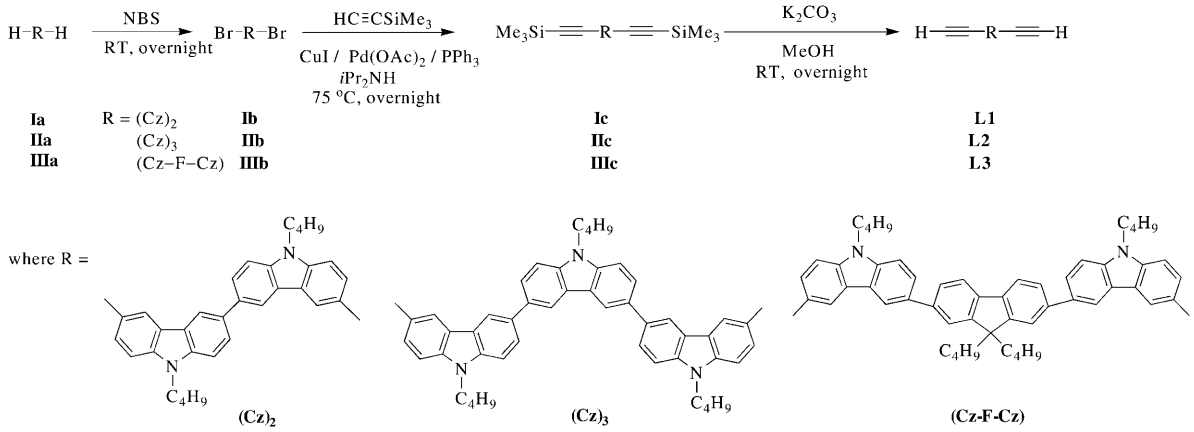

Scheme 2. Synthesis of diethynylated oligocarbazole and carbazole-fluorene ligands **L1**–**L3**. NBS = N-bromosuccinimide.

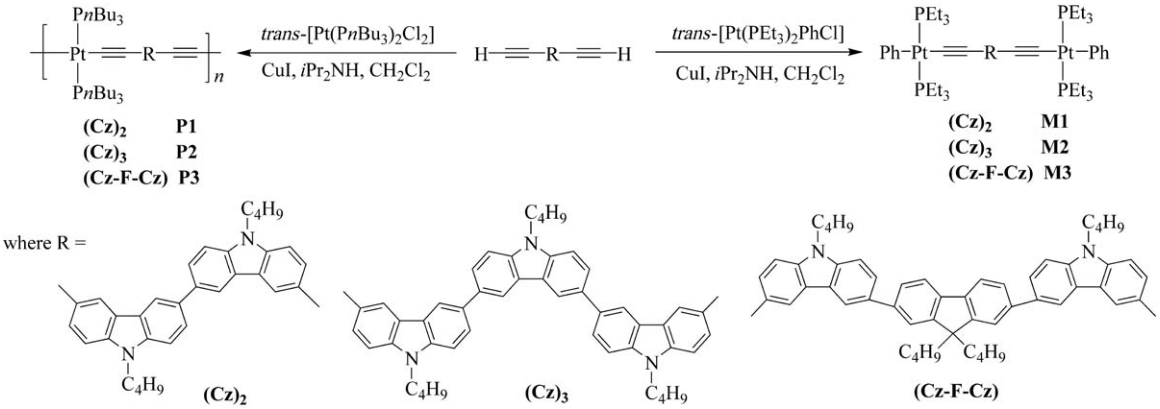

Scheme 3. Synthesis of Pt^{II} polyynes **P1**–**P3** and diynes **M1**–**M3**.

view that there is a high degree of polymerization in most of these polymers. The thermal properties of **P1**–**P3** were examined by thermal gravimetric analysis (TGA) under nitrogen. Analysis of the TGA trace (heating rate: 20 °C min^{-1}) for the polymers shows that they have onset decomposition temperatures (T_{decomp}) around 350 °C, indicative of their excellent thermal stability. Their degradation patterns are quite similar and we observe sharp weight losses of 31 to 35 %, corresponding to the elimination of PBu_3 and butyl groups from the polymers.

These new compounds were characterized by analytical and spectroscopic methods. The IR, NMR (^1H, ^{13}C, and ^{31}P), and mass spectral data shown in the Experimental Section are in accordance with their chemical structures. The solution IR spectra of these new metal complexes display a single sharp ν(C≡C) absorption band in the range of 2095–2099 cm^{-1}, consistent with a *trans* configuration of the ethynylene ligands around the metal center. The absence of the C≡CH stretching mode of each compound at around 3300 cm^{-1} indicates the formation of a M−C≡C bond. The NMR spectral data supported the conclusion that these compounds have well-defined and symmetrical structures. The ^{31}P NMR spectra of the Pt^{II} complexes exhibit a single resonance with a pair of Pt satellites, which confirms the *trans* arrangement of the phosphine ligands around platinum. The $^1J_{P,Pt}$ values in the Pt^{II} diynes (ca. 2629–2643 Hz) are typical of those found for related *trans*-PtP_2 systems.[12,13] Notably, two distinct ^{13}C NMR signals for the individual sp carbons in these complexes were observed, and they are shifted downfield with respect to the free ligands. The aromatic region of the ^{13}C NMR spectra also gives more precise information about the regiochemical structure of the main-chain skeleton and reveals a high degree of structural regularity in the polymers. As an example, only 12 well-defined peaks appear in the aromatic region, related to the 24 aromatic carbon atoms of the symmetric diplatinum structure for **P1**. The formulas of **M1**–**M3** were successfully established by the observation of intense molecular ion peaks in the positive-ion FAB mass spectra.

Photophysical properties

Establishment of the energy donor and acceptor: Because of the very strong overlap between the absorption component of the **Cz** and **F** chromophores, the establishment of the donor and acceptor is appropriately made on the basis of the fluorescence and phosphorescence spectra. Figure 1 shows the electronic spectra for **P1**, **P2**, **P3**, and **M3**.

The emission spectrum of **P1** exhibits a fluorescence band with some vibronic structure at 382 and 400 nm (for example), and a long tail in the red region associated with a weak phosphorescence. This spectrum bears similarities with that for **P2** where the fluorescence vibronic structures also show features at 380 and 400 nm. The phosphorescence portion of the spectrum in **P2** exhibits a relatively more intense luminescence with vibronic features starting at 488 nm. A comparison of the emission spectra of **P1** and **P2** allows one to address the effect of the addition of a **Cz** chromophore between the **Cz**-C≡C-PtL_2-C≡C-**Cz** units; the phosphorescence band is stronger in **P2**, very likely resulting from the central **Cz** fragment. **P3** exhibits a fluorescence ($\lambda_{(0-0)} = 404$ nm) and a phosphorescence ($\lambda_{(0-0)} = 540$ nm) that differs in band shape and position in comparison with that for **P1** and **P2**, demonstrating that these emissions arise from the **F** chromophore only.[14] The **Cz** luminescence is not observed, which indicates quenching of the **Cz** emission. Based on the position of the 0–0 fluorescence and phosphorescence peaks (Table 1 and Figure 1), one can readily predict the **Cz** and **F** chromophores as both singlet and triplet energy donor and acceptor, respectively (Figure 2). Evidence is provided below.

M1, **M2**, and **M3** exhibit fluorescence but not phosphorescence (see Table 1 and **M3** in Figure 1 as an example). The six compounds and polymers were also investigated at 77 K, because of the convenient increase in emission intensity and lifetimes (Table 3), giving access to the evaluation of energy transfer rates.

Figure 3 exhibits the electronic spectra of the polymers in 2MeTHF at 77 K, which exhibit better vibronically resolved bands. Based on the position of the 0–0 fluorescence and

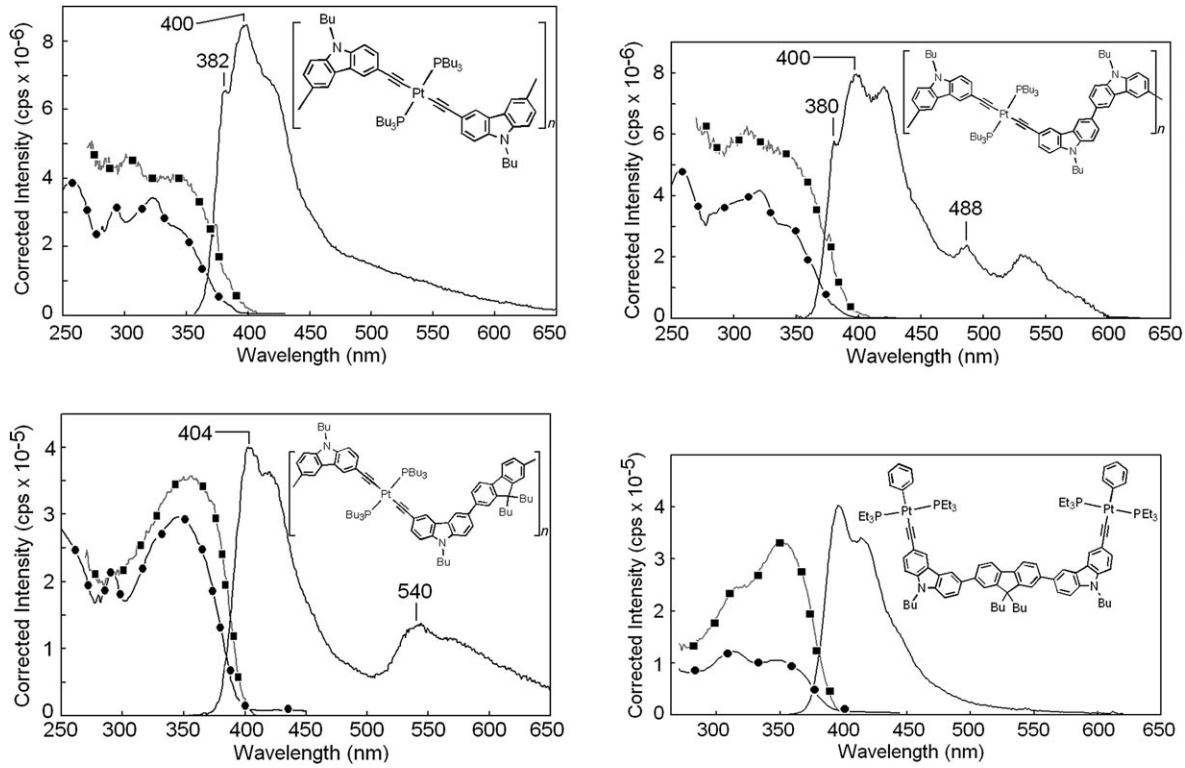

Figure 1. Absorption (●), emission (black line) and excitation spectra (■) of **P1** (top left), **P2** (top right), **P3** (bottom left) and **M3** (bottom right) in degassed 2MeTHF at 298 K.

Table 1. UV/Vis absorption and emission data and lifetimes at 298 K in degassed 2MeTHF.[a]

	Absorption λ [nm]	Fluorescence λ [nm]	Phosphorescence λ [nm]	Lumophore	τ_F [ns] ($\lambda_{obs.}$ [nm])	τ_P [μs] ($\lambda_{obs.}$ [nm])
M1	226, 258, 290, 310 sh, 325	350 sh, 415	–	**Cz**	0.160 ± 0.050 (417 nm)	–
M2	256, 320	370 sh, 420, 445 sh	–	**Cz**	0.130 ± 0.040 (420 nm)	–
M3	246, 256, 292, 325, 350	404, 420	–	**F**	0.120 ± 0.010 (400 nm)	–
P1	256, 282, 290, 324, 340 sh	382, 400, 420 sh, 450 sh	long tail at ca. 500	**Cz**	0.180 ± 0.030 (415 nm)	–
P2	258, 320, 350 sh	380, 400, 420	488, 530	**Cz**	0.070 ± 0.010 (415 nm)	–
P3	250, 294, 348	404, 420 sh	540, 565 sh	**F**	0.140 ± 0.020 (420 nm)	240 ± 20 (536 nm)

[a] sh = shoulder peak.

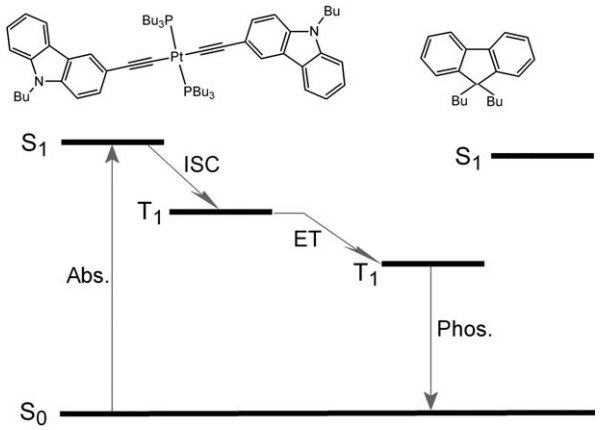

Figure 2. State diagram representing the **Cz**-C≡C-Pt(PBu_3)$_2$-C≡C-**Cz** fragment with respect to **F** chromophore useful for the analysis of the energy transfer processes in this work.

phosphorescence peaks, the assignment for both the singlet and triplet energy donor (**Cz**) and acceptor (**F**) is also confirmed at this temperature (see Table 2). As concluded for the 298 K data, **P3** and the model compound **M3** do not exhibit any evidence for fluorescence of the **Cz** chromophore at 77 K, indicating clear quenching. However, **P3** exhibits evidence of phosphorescence at 454 nm (narrow 0–0 peak) assigned to **Cz**. Unambiguous evidence for the existence of weak phosphorescence in **P3** and **M3** is provided by time-resolved spectroscopy in the μs time scale (where fluorescence has totally relaxed and is not present in the spectra). Figure 4 compares the time-resolved spectra of **P2** and **P3**, and **M2** and **M3**, where the **Cz** peak at 454 nm is observed in both **P2** and **P3**, and the peak at 450 nm in **M2** and **M3**. The presence of weak **Cz** phosphorescence indicates that the deactivation of the S_1 state of **Cz** (by intramolecular singlet electron transfer to the **F** residue; see below) competes

Table 2. UV/Vis absorption and emission data and T_1-T_1 transient lifetimes at 77 K in 2MeTHF.[a]

	Absorption λ [nm]	Fluorescence λ [nm]	Φ_F (± 10%)	Phosphorescence λ [nm]	Φ_P (±10%)[b]	Lumo-phore	τ_F [ns] ($\lambda_{obs.}$ [nm])	τ_P [μs] ($\lambda_{obs.}$ [nm])	τ_{trans} [μs] (±5%)
M1	268, 296, 310 sh, 326, 338 sh, 366 sh, 384 sh	395 sh, 415	0.0028	446, 478, 492	0.54	**Cz**	0.340 ± 0.050 (410)	147 ± 3 (446)	138
M2	258, 274 sh, 325, 338 sh, 366 sh, 384 sh	400 sh, 420	0.0021	447, 479, 491 sh	0.25	**Cz**	0.350 ± 0.025 (400)	149 ± 2 (447)	153
M3	260, 296, 325, 362, 380	399, 422, 447	0.17	522, 565, 600 sh	0.17 (**F**)	**Cz**	not observed	132 ± 6 (450)	–
						F	0.290 ± 0.025 (420)	175 ± 1 (522)	193
P1	284, 292, 326, 346, 360, 370	395, 422	0.0068	455, 477, 490, 504, 525 sh	0.49	**Cz**	0.215 ± 0.015 (420)	61 ± 1 (450)	74
P2	324, 348, 370	395, 420	0.0035	458, 483, 505, 540 sh	0.47	**Cz**	0.280 ± 0.020 (420)	66 ± 1 (450)	70
P3	288, 292, 360	401, 423	0.0077	454, 530, 570, 615 sh	0.14 (**F**)	**Cz**	not observed	52 ± 2 (450)	–
						F	0.290 ± 0.030 (423)	316 ± 23 (527)	329

[a] sh = shoulder peak. [b] The parentheses indicate which chromophore was monitored.

Table 3. Electrochemical properties of selected ligands and complexes.

Compound	E_{ox} [V][a]	E_{HOMO} [eV]	E_g [eV][b]	E_{LUMO} [eV][c]
L1	0.61	−5.41	3.73	−1.68
L2	0.54	−5.34	3.58	−1.76
L3	0.65	−5.45	3.20	−2.25
(Pt-(Cz)$_1$)$_n$[d]	0.41	−5.21	3.18	−2.03
P1	0.39	−5.19	3.19	−2.00
P2	0.36	−5.16	3.19	−1.97
P3	0.38	−5.18	3.12	−2.06

[a] 0.1 M $[Bu_4N]PF_6$ in CH_2Cl_2, scan rate 100 mV s^{-1}, versus Fc/Fc^+ couple. [b] Estimated from the onset wavelength of the solution-state optical absorption. [c] LUMO = HOMO + E_g. [d] The synthesis of this polymer has been reported previously, see reference [21].

with the intersystem crossing rate constant, without being significantly larger. For example, the intersystem crossing rate constant normally lies in the range between 10^{11} and 10^{12} s^{-1} for heavy-atom-containing aromatics.[14] This statement does not preclude the possibility of sensitization of the **Cz** triplet state by the **F** chromophore (S_1–T_1), although such an event is much less encountered.

Evidence for total quenching of the **Cz** fluorescence in **P3** and **M3** is provided by time-resolved spectroscopy during the rise time of the laser excitation pulse while excited at 340 nm (at this wavelength both chromophores, **Cz** and **F**, are excited; see Figure 5). At the beginning of the laser pulse (delay time = 43.5 ns), the signal intensity is very weak but the vibronic progression is perceptible. As the delay time increases, the intensity of the observed fluorescence expectedly increases, allowing one to monitor the peak positions and their relative intensities. For both **M3** and **P3**, the spectral signature is that of the **F** chromophore based on the peak positions. At further delay times (i.e. after the pulse maximum), the fluorescence intensities decrease and the band shape never changes for all delay times. No sign of the **Cz** fluorescence was observed for **M3** and **P3**.

Evidence for triplet energy and singlet electron transfer: Based on the position of the 0–0 peak observed in the fluorescence spectra, the upper energy donor (**Cz**) and lower energy acceptor (**F**) were assigned. The excitation spectrum of the fluorescence of **M3** monitored at 400, 420, 450, and 475 nm (i.e. where only **F** is emitting) exhibits a low-energy and redshifted peak at 390 nm (gray line), along with a series of higher energy bands (Figure 6). Based on the absorption spectrum of Figure 3 (and the data of Table 1), the observed 0–0 peak is located at 380 nm. This observation indicates that the observed **F** fluorescence arises from the red-

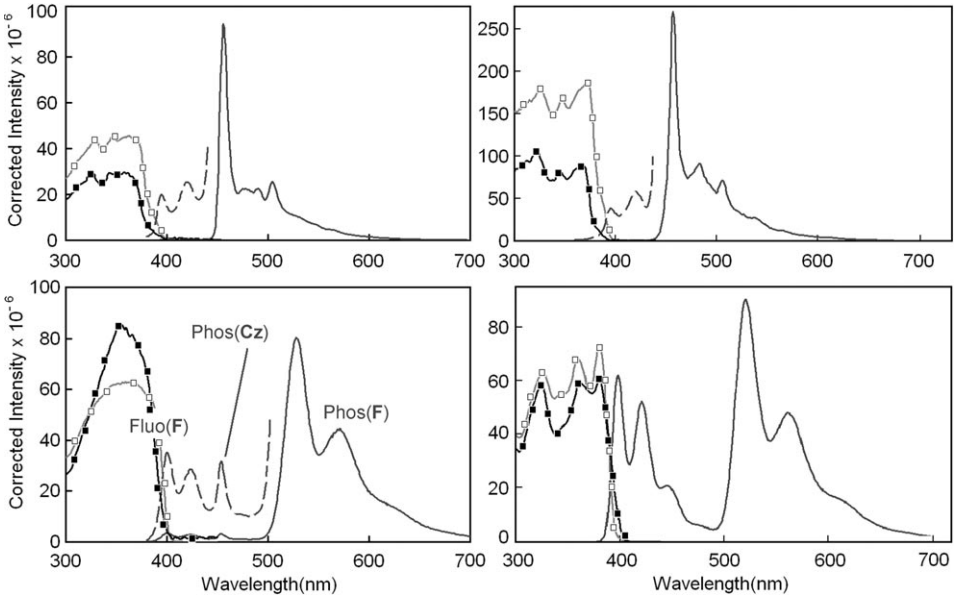

Figure 3. Absorption (■), emission (black line) and excitation spectra (□) of **P1** (top left), **P2** (top right), **P3** (bottom left) and **M3** (bottom right) in degassed 2MeTHF at 77 K. Fluo = fluorescence; Phos = phosphorescence. For **P2** and **P3**, the blue-shifted emissions (dashed line) are multiplied by 100 and 20, respectively.

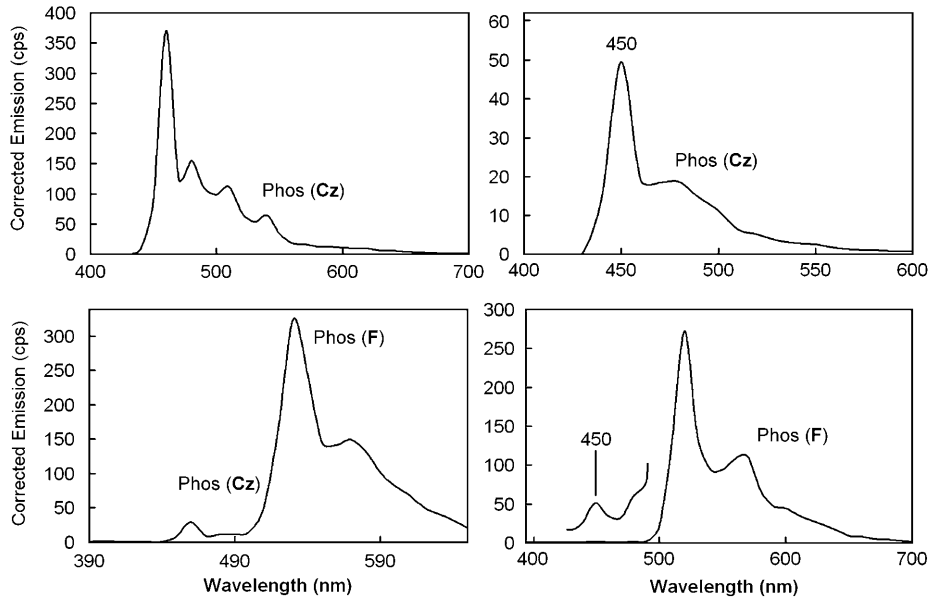

Figure 4. Time-resolved emission spectra of **P2** (top left), **P3** (bottom left), **M2** (top right), and **M3** (bottom right) in 2MeTHF at 77 K in the 10–50 μs time scale. The phosphorescence of the carbazole and fluorene chromophores is indicated as Phos (**Cz**) and (**F**), respectively.

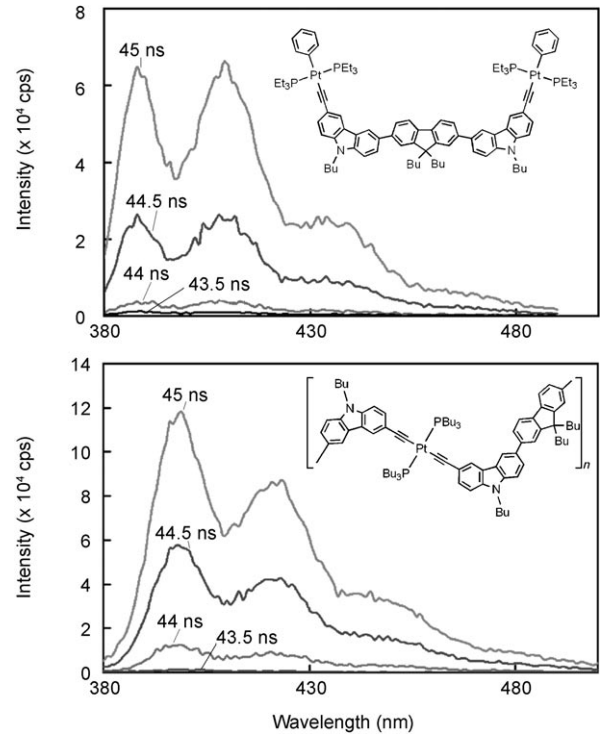

Figure 5. Time-resolved fluorescence spectra of **M3** (top) and **P3** (bottom) in 2MeTHF at 77 K. The time delays are indicated on the graphs and correspond to the rising time of the laser pulse where the delay time of 43.5 ns is the beginning of the laser pulse and the delay time of 45 ns is the pulse maximum (λ_{exc} = 340 nm). The pulse width at half maximum is 1.3 ns.

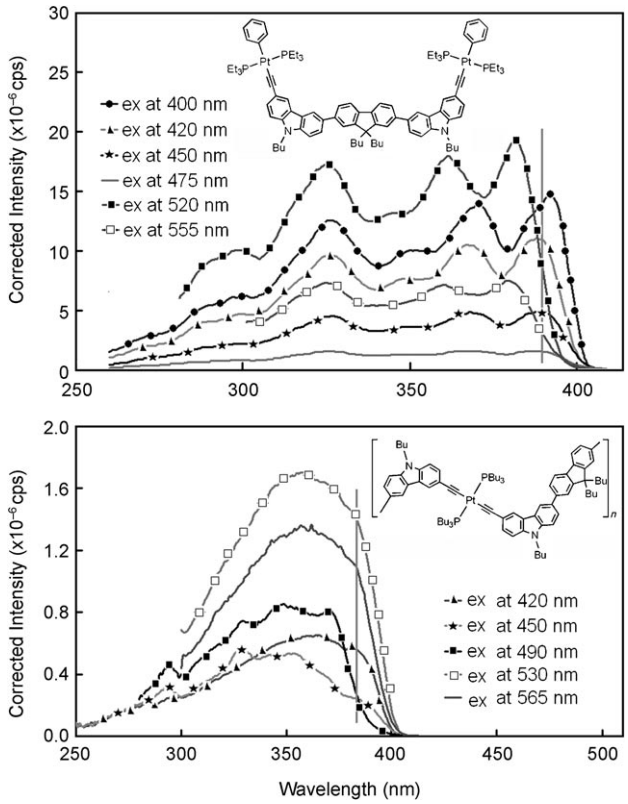

Figure 6. Excitation spectra of **M3** and **P3** in 2MeTHF at 77 K monitored at different wavelengths. The grey lines represent a comparison mark of the 0–0 peak of **F** with respect to the rest of the spectra.

arising from the **F** chromophore), the excitation spectrum becomes different, resembling more the observed absorption spectrum (Figure 3). This result indicates that both chromophores (since the absorption is composed of both units), but primarily the **Cz** (since it is significantly different from the excitation spectrum with λ_{obs} = 400, 420, 450, and 475 nm), populate the lower-lying triplet emissive state of **F**. Triplet energy transfer **Cz**→**F** confirms this (Figure 7).

While the exact individual absorption profile for **Cz** and **F** is unknown (and there is no way of knowing because of the conjugation between the two chromophores), it is not possible to quantify the ratio of shifted absorption system, which is that of **F** as well. Monitoring at 520 and 555 nm (i.e. in the phosphorescence band phosphorescence arising from the T_1(**F**) and T_1(**Cz**) states. Because of this uncertainty, it is also not possible to state

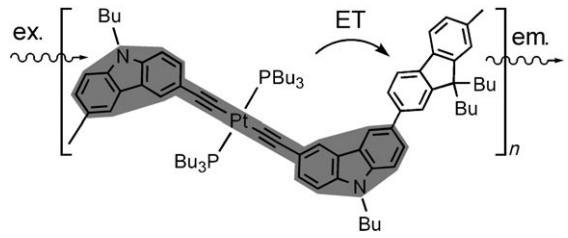

Figure 7. Simplified representation of triplet energy transfer in organometallic [-D-A-D-]$_n$ systems. Transfers to both neighboring chromophores are possible. Only one is shown for clarity.

with this experiment whether the **Cz** unit contributes to the fluorescence of **F** in **M3** (i.e. singlet–singlet energy transfer), but the difference in excitation spectra monitored at 400, 420, 450, and 475 nm, representing the **F** unit, with that of 520 and 555 nm, representing mostly **Cz**, is striking. The excitation spectra monitored in the **F** fluorescence band are those of the **F** chromophore only, whereas those monitored in the **F** phosphorescence are those of the **Cz** one (mostly). Thus, it appears that the singlet–singlet energy transfer from **Cz** to **F** is relatively inefficient, which strongly argues in favor of a photo-induced electron transfer process to explain the *total absence* of **Cz** fluorescence in **M3** and **P3**. Based on this argument and by analogy with other **Cz**–**F** systems,[9,10] the quenching of the **Cz** fluorescence is assigned to an electron transfer from the S_1 state of **Cz** to **F**.

The emission spectrum of **P3** monitored at 420 nm exhibits a slightly redshifted signal with respect to the absorption band (Figure 3), indicating also that the **F** unit contributes to the observed fluorescence (of **F**). At 450 nm, a signal associated with the **Cz** phosphorescence superimposed the fluorescence. The excitation spectrum monitored at this wavelength resembles that of the absorption, indicating that both **Cz** and **F** units contribute to the overall intensity at 450 nm, consistent with the nature of the emitted light. At 490 nm where the fluorescence and phosphorescence of **F** is almost of no intensity, the excitation spectrum (black line) differs from both the excitation and absorption, strongly suggesting that the signature is that of the **Cz** mostly. This is indeed confirmed by comparing this excitation spectrum to that of the absorption spectra of **P1** and **P2** (Figure 3) for which no **F** absorption occurs. The excitation spectra monitored at 530 and 565 nm (in the phosphorescence of the **F** unit), exhibit a band shape similar to the absorption, except that the low-energy signal (i.e. presumably the 0–0 peak of **F**) is better defined. All in all, the phosphorescence of **F** in **P3** arises from both the **Cz** (via triplet–triplet energy transfer) and **F** (via intersystem crossing) moieties.

Evidence for triplet–triplet energy transfer is also provided from the transient spectra. The triplet–triplet absorption processes for **Cz** and **F** are known.[9,10] In the presence of triplet energy transfer, the triplet–triplet absorption is still present, but in the presence of an efficient electron transfer the triplet–triplet signature should vanish and be replaced by an absorption band related to a charge-separated state; in this work, $\mathbf{F}^-$ ion (i.e. fluorene anion) and [**Cz**-C≡C-Pt-$(PEt_3)_2$-C≡C-**Cz**]$^+$ ion. Figure 8 exhibits the ns transient spectra of **M2**, **P2**, **M3**, and **P3**, which are all very similar to the triplet–triplet transient spectra of **Cz** and **F**,[9,10] which witness the presence of these species lying in their triplet states. No other band was observed, indicating that no charge-separated state was detected in this time scale.

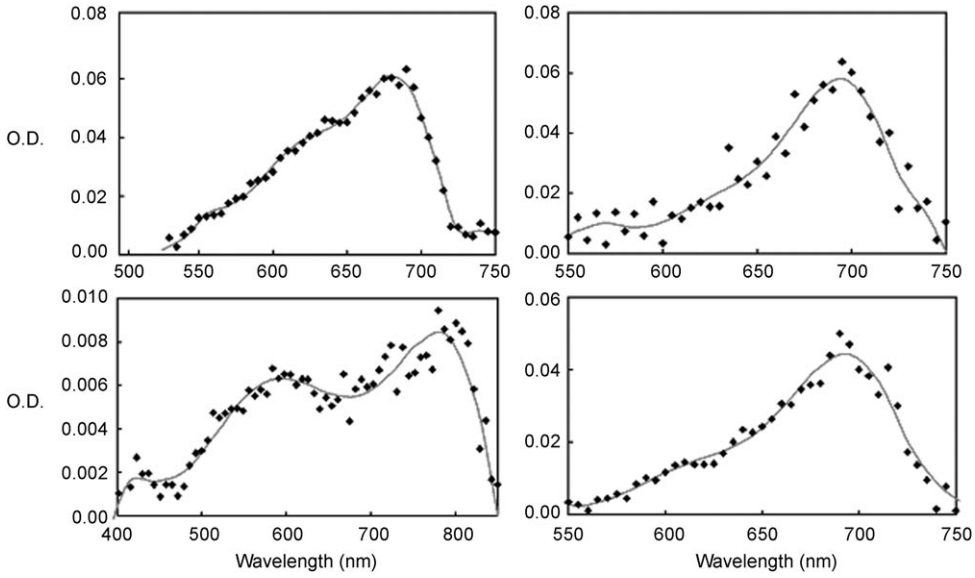

Figure 8. Transient spectra of **M2** (top left) and **P2** (bottom left) in the 8–65 μs time scale and **M3** (top right) and **P3** (bottom right) in 2MeTHF at 77 K excited at 355 nm in the 8–60 μs time scale.

An investigation of the concentration effect on the emission band in the range 1.8×10^{-6} to 4.4×10^{-7} M for **P3** and 2.2×10^{-7} to 1.2×10^{-5} M for **M3** (typical concentrations in this work) was performed to insure that no aggregation phenomenon was observed. The resulting emission bands did not change in position, shape, and relative intensity ratio.

Evidence for conjugation: Unambiguous evidence for conjugation across the polymer chain is provided by the comparison of the electronic spectra of compound **IIIa** (Figure 9), a precursor presented in Scheme 2, with that of **M3** and **P3** (Figure 3 and Table 1). At 77 K, compound **IIIa** does not exhibit phosphorescence, a process that is strongly promoted by spin-orbit coupling due to the presence of Pt. In **M3** and **P3**, phosphorescence due to the **F** chromophore is the stron-

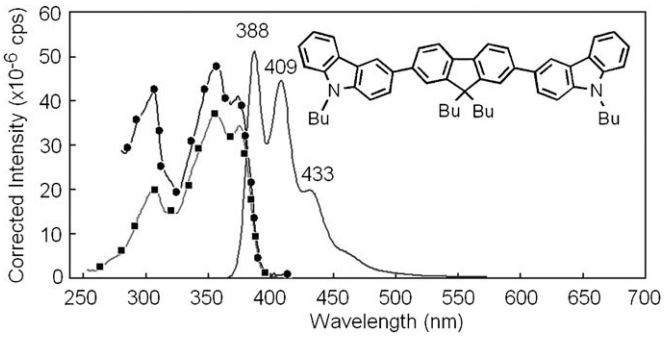

Figure 9. Absorption (●), emission (black line), and excitation spectra (■) of **IIIa** in 2MeTHF at 77 K (i.e. under the same experimental conditions as in Figure 3).

gest signal. In addition, the peak positions for the fluorescence are 399 and 422 nm for **M3** and 401 and 423 nm for **P3**. These values are redshifted with respect to **IIIa** (388 and 409 nm; Figure 9). Both the redshift of the **F** fluorescence and the enhancement of the phosphorescence intensity due to intersystem crossing clearly demonstrate conjugation in the Pt compounds.

Molecular orbital considerations: The frontier MOs are addressed by density functional theory (DFT) calculations using an optimized geometry for **Cz**-≡-PtL_2-≡-**Cz**-**F**-**Cz**-≡-PtL_2-≡-**Cz** as a model (Figure 10). The degenerate HOMO

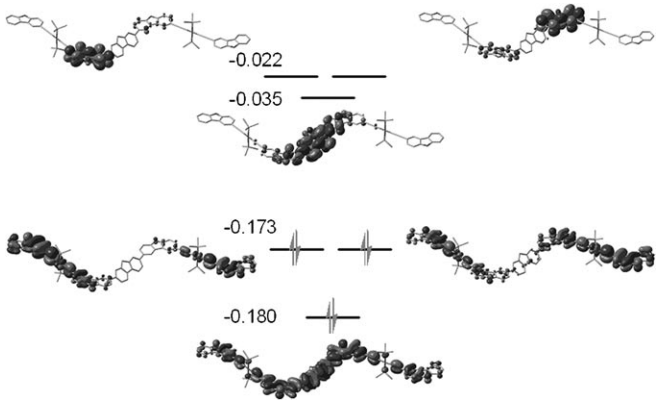

Figure 10. MO representations of the frontier MOs of a model compound **Cz**-≡-PtL_2-≡-**Cz**-**F**-**Cz**-≡-PtL_2-≡-**Cz**. The energies are in a.u. (1 a.u. = 27.2114 eV).

(together with HOMO−1) and the nondegenerate HOMO−2 exhibit atomic contributions for a π system distributed over the **Cz**-≡-PtL_2-≡-**Cz** units in all cases, which is consistent with this type of chromophore (Ph-≡-PtL_2-≡-Ph).[14c] This degeneracy is anticipated due to the identical nature of the units. In addition, the HOMO−2 also exhibits an atomic contribution over the **F** chromophore, consistent with the experimentally demonstrated conjugation in the backbone, but does not show a Pt contribution. Instead, the n-lone pairs of the P atoms, symmetrically appropriate for the π system, are also computed.

The LUMO is also a π system localized primarily over the **F** residue with some atomic contribution placed on the neighboring C atoms of both **Cz** units. This not only indicates the presence of weak conjugation over the **Cz**-**F**-**Cz** fragment, but also the presence of a rather localized excited state. The LUMO+1 and LUMO+2 exhibit π systems localized almost exclusively on the **Cz** unit, suggesting strong localization of the upper excited states (i.e. S_2 and T_2). All in all, the nature of these polyaromatic materials in their ground state is conjugated, whereas the two lowest energy excited states are localized.

Next, time-dependent DFT (TDDFT) was used to address the nature of the lowest energy electronic transition, and consequently the nature of the corresponding excited state. The computed transition energy (0–0) is 359.5 nm, which compares favorably with the 0–0 signal depicted (as a shoulder) in the absorption spectra at 77 K for **M3** and **P3** (in the 360–380 nm range; Table 3). The computed oscillator strength (*f*) is 1.13, indicating that the transition is allowed, consistent with the observation. This transition is composed of two components; HOMO−2/LUMO and HOMO/LUMO with a coefficient of 0.570 and 0.349, respectively. This result corroborates that the low-energy excited state exhibits charge-transfer character of the type **Cz**-≡-PtL_2-≡-**Cz**→**F**, including the HOMO→LUMO as well as the HOMO−2→LUMO transitions; the latter component being the major component.[16]

Rates for triplet energy and singlet electron transfers at 77 K: The rate of triplet energy transfer (k_{ET}) is given by $k_{ET}=(1/\tau_e)-(1/\tau_e^0)$,[17] where τ_e and τ_e^0 are the emission lifetimes for the **D**–**A** dyad and a closely related compound in which no energy transfer takes place. For **P3** ($\tau_e^0=52\pm2$) and **M3** (132 ± 6), **P2** (66 ± 6) and **M2** (175 ± 1 μs) were used as comparative species, respectively. Hence, the triplet k_{ET} values are about 1.9×10^3 and 3.4×10^3 s^{-1} for **M3** and **P3**, respectively. Taking into account the uncertainties, the lower and upper limits for k_{ET} for **M3** are 1.5×10^3 and 2.3×10^3 s^{-1}, and for **P3** are 1.4×10^3 and 5.1×10^3 s^{-1}. The larger triplet k_{ET} for **P3** (excluding the uncertainties) agrees with a larger number of pathways for energy transfers (one chromophore on each side of the **Cz**) with respect to **M3** (only one).

While these k_{ET} values compare favorably with those of other triplet energy transfer systems,[17] these values lie on the lower end of the literature data.[18] This is due to the fact that only the short distance Dexter mechanism operates in the triplet states,[17] a process that involves a dual electron transfer and therefore **D**–**A** orbital overlap. Owing to the nonzero dihedral angle between **Cz** and **F**, these overlaps are poorer (in comparison with fully conjugated planar systems, or **D**-≡-**A** for instance).[18]

A close examination of the fluorescence decay traces of **M3** and **P3** indicates the presence of a single exponential, meaning that the observed emissions arise from the **F** lumophore only. Again, the **Cz** fluorescence is either totally quenched or much too weak to be observed, which illustrates efficient singlet electron transfer (^{1}**Cz***→**F**). The lack

of τ_F(**Cz**) precludes an accurate evaluation of the rate of electron transfer, singlet k_{et}. By using the limit of our emission detection ($\Phi_F < 0.0001$), and $k_{et} = (\Phi_F^0/\tau_F^0)[(1/\Phi_F)(1/\Phi_F^0)]$,[18] where Φ_F and Φ_F^0 are the fluorescence quantum yields for the donor in the dyad **D**–**A** and the model compounds in which no electron transfer takes place (i.e. **M1** ($\Phi_F^0 = 0.033$ at $\lambda_{exc} = 340$ nm) and **P1** ($\Phi_F^0 = 0.0082$ at $\lambda_{exc} = 340$ nm with respect to 9,10-diphenylanthracene; $\Phi_F = 1.0$[19])), one can evaluate the lower limit for singlet k_{et} (**M3**, $k_{et} > 10 \times 10^{11}\ s^{-1}$; **P3**, $k_{et} > 4 \times 10^{11}\ s^{-1}$). These singlet k_{et} values occurring in the low ps time scale are comparable with other rates measured for charge-separated states of various dyads.[18] In addition, the fact that a little bit of **Cz** phosphorescence was observed for **M3** and **P3** suggesting that k_{et} competed (same order of magnitude) with the rate for intersystem crossing (normally in the 10^{11}–$10^{12}\ s^{-1}$ time scale),[15] indicates that the calculated limits for k_{et} shown above must be close to the real values.

M2 and **P2**, in which three **Cz** units are connected together, were studied as well. The similarity in spectroscopic and photophysical data (i.e. fluorescence and phosphorescence lifetimes) between **M1** and **M2** and **P1** and **P2** reveals the absence of singlet and triplet quenching no matter whether there are two or three **Cz** units. This observation indicates no singlet electron transfer and triplet energy transfer between the adjacent **Cz** and the central **Cz** in **M2** and **P2**. No triplet energy transfer rate could be measured at room temperature since no **Cz** phosphorescence could be detected.

Electrochemical findings: Cyclic voltammetry provides additional data regarding the thermodynamic driving forces for the electron transfer process. The oxidation potentials measured for **L1** and **L2** (Table 3) are consistent with the presence of conjugation. For instance, the decrease in oxidation potential on going from **L1** to **L2** indicates the presence of an extended conjugation in **L2** (two **Cz** units for **L1** and three **Cz** units for **L2**). Also, the increase in oxidation potentials on going from **L2** to **L3** is consistent with the fact that **F** is harder to oxidize than **Cz**, which also indicates that **Cz** is more prone to act as an electron donor than **F**. A comparison of the oxidation potentials between **Ln** and **Pn** (**n** = 1–3) and polymer (-C≡C-PtL_2-C≡C-**Cz**-)$_n$ (abbreviated as **(Pt-(Cz)$_1$)$_n$**) indicates a decrease in value for the polymers, which is in agreement with the extension of the conjugation. The relative tendency observed for **L1** to **L3** is also seen in **P1** to **P3**. All in all, the **Cz** center is the most likely unit prone to oxidation, which agrees totally with the DFT findings (see the degenerate HOMO and HOMO−1). These same calculations indicate that **F** is the most likely candidate for reduction, in line with the electron transfer mechanism occurring in the singlet state. No reduction wave was observed within the electrochemical window of the solvent used.

Comments on singlet electron transfer versus triplet energy transfer: In a recent paper dealing with dendrimers of carbazoles having norbornadiene (**NBD**) as a central core (where **Cz** and **NBD** are not conjugated), the conversion of singlet electron transfer at room temperature versus triplet energy transfer at 77 K was demonstrated.[9] The time scale for these events is 0.4×10^8 to $1.8 \times 10^9\ s^{-1}$ for the electron transfer at room temperature and 0.08 to $0.96\ s^{-1}$ for triplet energy transfer at 77 K. These rates are much slower than those reported in this work and are consistent with the presence (fast) or absence (slow) of conjugation. The shut down of the electron transfer at low temperature comes from the large solvent reorganization energy in frozen media. In this work, the total quenching of the **Cz** fluorescence in **M3** and **P3** is obvious. Therefore, a "shut down" mechanism was not observed since total quenching of the **Cz** fluorescence was observed at both temperatures. The reason for this most likely comes from the fact that the oligomer **M3** and the polymer **P3** are conjugated and so the cationic and anionic charges are distributed over a large number of atoms.

Concluding Remarks

This work reports the first example of quantified intrachain electron transfer (inducing fluorescence quenching of **D**) and energy transfer in conjugated organometallic polymers. The rates are fast and slow for singlet electron transfer and triplet energy transfer, respectively. From the detailed emission spectral assignment, we can regard the **Cz** and **F** chromophores as both singlet and triplet energy donor and acceptor, respectively. Apparently, k_{ET} is larger for **P3** than for **M3** due to the number of possible sites for triplet energy transfer, thus the photophysics of polymers are intrinsically bound to differ from short-chain molecules. Remarkably, intramolecular photophysical processes can influence the resulting emission intensity of the various aryl fragments in metallopolyynes. Based on the recorded spectra, it becomes evident that depending on the selected aromatics, the intensity of both the fluorescence and phosphorescence can be adjusted. In this way, one can cover the whole visible spectrum (380–720 nm), hence inducing white light emission, a much desired color for light-emitting diodes currently. Such an approach will have an important impact on the way researchers think in the design of novel metal-containing conjugated polymers for future practical optoelectronic applications.

Experimental Section

General: All reactions were carried out under a nitrogen atmosphere by using standard Schlenk techniques. Solvents were predried and distilled from appropriate drying agents under an inert atmosphere prior to use. Glassware was oven-dried at about 120 °C. All reagents and chemicals, unless otherwise stated, were purchased from commercial sources and used without further purification. The compounds 9-butylcarbazole-3-boronic acid,[11d,20] 3,6-dibromo-9-butylcarbazole,[21] 2,7-dibromo-9,9-dihexylfluorene,[21] *trans*-[Pt(PEt_3)$_2$PhCl],[22] and *trans*-[Pt($PnBu_3$)$_2$$Cl_2$][23] were prepared according to the literature methods. Preparative TLC

(20 cm × 20 cm) was performed on 0.7 mm silica plates (Merck Kieselgel 60 GF_{254}) prepared in our laboratory.

Instrumentation: Infrared spectra were recorded as CH_2Cl_2 solutions using a Perkin–Elmer Paragon 1000 PC or Nicolet Magna 550 Series II FTIR spectrometer, using CaF_2 cells with a 0.5 mm path length. NMR spectra were measured in appropriate deuterated solvents on a JEOL EX270 or a Varian Inova 400 MHz FT-NMR spectrometer, with ^1H NMR chemical shifts quoted relative to $SiMe_4$, and ^{31}P chemical shifts relative to an 85% H_3PO_4 external standard. Fast-atom bombardment (FAB) mass spectra were recorded on a Finnigan MAT SSQ710 mass spectrometer in *m*-nitrobenzyl alcohol matrices. The molecular weights of the polymers were determined by GPC (HP 1050 series HPLC with visible wavelength and fluorescent detectors) using polystyrene standards and THF as eluent, and the thermal analyses were performed with the Perkin–Elmer TGA6 thermal analyzer. The UV/Vis spectra were recorded on a Hewlett-Packard diode array model 8452 A at Sherbrooke. The emission and excitation spectra were obtained by using a double monochromator Fluorolog 2 instrument from Spex. Phosphorescence time-resolved measurements were performed on a PTI LS-100 using a 1 μs tungsten flash lamp. Fluorescence and phosphorescence lifetimes were measured on a Timemaster Model TM-3/2003 apparatus from PTI. The source was a nitrogen laser with a high-resolution dye laser (FWHM ≈1.5 ns), and the fluorescence lifetimes were obtained from high-quality decays and deconvolution or distribution lifetime analysis. The uncertainties were about ±40 ps based on multiple measurements. The flash photolysis spectra and the transient lifetimes were measured with a Luzchem spectrometer using the 355 nm line of a YAG laser from Continuum (Serulite), and the 355 nm line from a OPO module pump by the same laser (FWHM = 13 ns).

Quantum yield measurements: For room-temperature measurements, all samples were prepared under an inert atmosphere (in a glove box, P_{O_2} < 20 ppm) by dissolution of the different compounds in 2MeTHF using 1 mL quartz cells with septum (298 K) or quartz NMR tubes in liquid nitrogen for 77 K measurements. Three different measurements (i.e. different solutions) were performed for each set of photophysical data (quantum yields, Φ_F and Φ_P). The sample concentrations were chosen to correspond to an absorbance of 0.05 at the excitation wavelength. Each absorbance value was measured five times for better accuracy in the measurements of emission quantum yield (Φ_e). The reference for Φ_e was 9,10-diphenylanthracene ($\Phi_F = 1.0$).[19]

Theoretical computations: Calculations were performed on an Intel Xeon 3.40 GHz PC with the Gaussian 03 revision C.02 and Gausview 3.0 software package. The hybrid B3LYP exchange-correlation function was used.[24–26] LANL2DZ pseudo-potentials and basis sets were used for platinum, 3–21G* pseudo-potentials for phosphorus, and 3–21G* basis sets for all atoms[27,28] except for platinum. The platinum structure file was optimized before the TDDFT calculation. Only the relevant (stronger oscillator strength and wavefunction coefficients) molecular orbitals are shown.

Electrochemical measurements: Electrochemical measurements were made using a Princeton Applied Research (PAR) model 273 A potentiostat. A conventional three-electrode configuration consisting of a glassy carbon working electrode, and Pt wires as both the counter and reference electrodes was used. The supporting electrolyte was 0.1 M $[Bu_4N]PF_6$. Ferrocene was added as an internal standard after each set of measurements, and all potentials reported were quoted with reference to the ferrocene–ferrocenium (Fc/Fc^+) couple at a scan rate of 100 mV s^{-1}. The oxidation potentials (E_{ox}) were used to determine the HOMO energy levels using the equation $E_{HOMO} = (E_{ox} + 4.8)$ eV, and the LUMO energy levels were determined from $E_{LUMO} = (E_{HOMO} + E_g)$ eV, where the ferrocene value lies at −4.8 eV with respect to the vacuum.[29]

Syntheses

The syntheses of **L1**–**L3** are given in the Supporting Information.

Synthesis of P1: A mixture of *trans*-$[Pt(PnBu_3)_2Cl_2]$ (100 mg, 0.150 mmol) and one equivalent of **L1** (73 mg, 0.150 mmol) was dissolved in iPr_2NH/CH_2Cl_2 (40 mL, 1:1, v/v), and CuI (5.0 mg) was subsequently added. After the mixture was stirred overnight at room temperature, all volatile components were removed under reduced pressure. The residue was redissolved in CH_2Cl_2 and the mixture was filtered through a short column using pure CH_2Cl_2 as eluent to give a brown solution of the polymeric material. After removal of the solvent by using a rotary evaporator, a brown powder was obtained. Further purification can be accomplished by precipitating the polymer solution in CH_2Cl_2 from MeOH to afford pure **P1** (91 mg, 59%). IR (CH_2Cl_2): $\tilde{\nu}$ = 2099 ν(C≡C) cm^{-1}; ^1H NMR ($CDCl_3$): δ = 8.31–8.02 (m, 4H, Ar), 7.73–7.14 (m, 8H, Ar), 4.20 (m, 4H, CH_2), 2.19 (m, 12H, CH_2), 1.79–1.30 (m, 32H, CH_2), 0.95–0.86 ppm (m, 24H, CH_3); ^{13}C NMR ($CDCl_3$): δ = 139.64, 139.00, 132.78, 128.77, 124.68, 122.76, 122.44, 119.82, 118.80, 118.06, 109.30, 108.76 (Ar), 108.51, 77.29 (C≡C), 42.92, 29.64, 26.07, 23.96, 21.97, 21.96, 13.97, 13.92 ppm (Bu); $^{31}P\{^1H\}$ ($CDCl_3$): δ = 3.89 ppm ($^1J_{Pt,P}$ = 2362 Hz); elemental analysis calcd (%) for $(C_{60}H_{84}N_2P_2Pt)_n$: C 66.09, H 7.77, N 2.57; found: C 65.89, H 7.66, N 2.42; GPC (THF): M_w = 10700, M_n = 8590, PDI = 1.25; TGA: T_{decomp}: 348 ± 5 °C.

Synthesis of P2: CuI (5.0 mg) was added to a mixture of **L2** (89 mg, 0.125 mmol) and *trans*-$[Pt(PnBu_3)_2Cl_2]$ (84 mg, 0.125 mmol) in iPr_2NH/CH_2Cl_2 (40 mL, 1:1, v/v). After the same workup procedure as described above, the polymer was isolated as a brown powder in 56% yield (92 mg). IR (CH_2Cl_2): $\tilde{\nu}$ = 2098 ν(C≡C) cm^{-1}; ^1H NMR ($CDCl_3$): δ = 8.46 (s, 2H, Ar), 8.32 (s, 2H, Ar), 8.10 (m, 2H, Ar), 7.81 (m, 5H, Ar), 7.53–7.43 (m, 7H, Ar), 4.29 (m, 6H, CH_2), 2.23 (m, 12H, CH_2), 1.87 (m, 6H, CH_2), 1.67–1.49 (m, 30H, CH_2), 0.99–0.89 ppm (m, 27H, CH_3); ^{13}C NMR ($CDCl_3$): δ = 140.06, 139.95, 139.77, 138.97, 133.43, 133.11, 129.02, 125.26, 123.62, 123.49, 123.20, 122.85, 119.86, 118.89, 111.97, 109.24, 109.14, 108.98 (Ar), 108.23, 77.32 (C≡C), 43.11, 29.69, 26.09, 23.97, 21.99, 20.64, 14.12, 13.91 ppm (Bu); $^{31}P\{^1H\}$ ($CDCl_3$): δ = 3.89 ppm ($^1J_{Pt,P}$ = 2358 Hz); elemental analysis calcd (%) for $(C_{76}H_{99}N_3P_2Pt)_n$: C 69.59, H 7.61, N 3.20; found: C 69.43, H 7.76, N 3.30; GPC (THF): M_w = 45930, M_n = 34410, PDI = 1.33; TGA: T_{decomp}: 350 ± 5 °C.

Synthesis of P3: This polymer was prepared similarly from **L3** (81 mg, 0.105 mmol) and *trans*-$[Pt(PnBu_3)_2Cl_2]$ (70 mg, 0.105 mmol) and it was isolated as a pale brown powder in 57% yield (82 mg) after being purified by the precipitation method. IR (CH_2Cl_2): $\tilde{\nu}$ = 2099 ν(C≡C) cm^{-1}; ^1H NMR ($CDCl_3$): δ = 8.32 (s, 2H, Ar), 8.13 (s, 2H, Ar), 7.81–7.69 (m, 8H, Ar), 7.44 (m, 4H, Ar), 7.29 (m, 2H, Ar), 4.30 (m, 4H, CH_2), 2.26 (m, 16H, CH_2), 1.88–1.53 (m, 32H, CH_2), 1.26–0.73 ppm (m, 38H, CH_2CH_3); ^{13}C NMR ($CDCl_3$): δ = 151.57, 140.86, 140.11, 139.39, 138.81, 132.57, 129.10, 126.00, 125.04, 123.28, 123.16, 122.80, 122.61, 121.52, 119.99, 119.81, 118.63, 109.22 (Ar) 108.83, 108.31 (C≡C), 55.14 (quat. C), 42.96, 40.46, 31.07, 29.34, 26.30, 24.35, 24.00, 23.83, 22.67, 20.55, 14.10, 13.89 ppm (Bu); $^{31}P\{^1H\}$ ($CDCl_3$): δ = 3.95 ppm ($^1J_{Pt,P}$ = 2357 Hz); elemental analysis calcd (%) for $(C_{81}H_{108}N_2P_2Pt)_n$: C 71.18, H 7.96, N 2.05; found: C 71.29, H 7.76, N 2.32; GPC (THF): M_w = 21190, M_n = 15890, PDI = 1.33; TGA: T_{decomp}: 348 ± 5 °C.

Synthesis of M1: The dehydrohalogenation reaction of **L1** (23 mg, 0.047 mmol) with two molar equivalents of *trans*-$[Pt(PEt_3)_2Cl(Ph)]$ (51 mg, 0.094 mmol) in the presence of CuI (3.0 mg) in iPr_2NH/CH_2Cl_2 (40 mL, 1:1, v/v) afforded the title complex as a white solid in 21% yield (15 mg) after the usual workup by TLC on silica using CH_2Cl_2/hexane (2:1, v/v) as eluent. IR (CH_2Cl_2): $\tilde{\nu}$ = 2096 ν(C≡C) cm^{-1}; ^1H NMR ($CDCl_3$): δ = 8.33 (s, 2H, Ar), 8.09 (s, 2H, Ar), 7.77 (d, J = 8.1 Hz, 2H, Ar), 7.45–7.24 (m, 10H, Ph + Ar), 6.95 (t, J = 8.1 Hz, 4H, Ph), 6.79 (t, J = 8.1 Hz, 2H, Ph), 4.29 (t, J = 16.2 Hz, 4H, CH_2), 1.81–1.61 (m, 28H, CH_2 of Et + CH_2 of Bu), 1.41–1.39 (m, 4H, CH_2), 1.17–0.92 ppm (m, 42H, CH_3 of Et + CH_3 of Bu); ^{13}C NMR ($CDCl_3$): δ = 156.83, 139.72, 139.29, 138.72, 133.32, 129.22, 127.19, 125.33, 123.27, 122.86, 122.39, 121.05, 120.03, 119.02, 110.58, 108.91 (Ar), 108.25, 108.69 (C≡C), 42.92, 31.19, 20.56, 13.90 (Bu), 15.11, 8.07 ppm (Et); $^{31}P\{^1H\}$ ($CDCl_3$): δ = 10.99 ppm ($^1J_{Pt,P}$ = 2643 Hz); FAB-MS: *m/z*: 1508 [M^+]; elemental analysis calcd (%) for $C_{72}H_{100}N_2P_4Pt_2$: C 57.36, H 6.69, N 1.86; found: C 57.20, H 6.53, N 1.95.

Synthesis of M2: Similar to **M1**, this complex was prepared from **L2** (23 mg, 0.033 mmol) and purified on preparative TLC plates with CH_2Cl_2/hexane (2:3, v/v) as eluent to give an oily solid in an isolated yield of 30% (17 mg). IR (CH_2Cl_2): $\tilde{\nu}$ = 2097 ν(C≡C) cm^{-1}; ^1H NMR ($CDCl_3$): δ = 8.47 (s, 2H, Ar), 8.34 (s, 2H, Ar), 8.07 (s, 2H, Ar), 7.80 (t, J = 8.1 Hz, 4H, Ar), 7.53–7.24 (m, 10H, Ph + Ar), 6.94–6.78 (m, 8H, Ph

+ Ar), 4.29 (m, 6H, CH_2), 1.81–1.61 (m, 30H, CH_2 of Et + CH_2 of Bu), 1.45–1.42 (m, 6H, CH_2), 1.16–0.92 ppm (m, 45H, CH_3 of Et + CH_3 of Bu); ^{13}C NMR ($CDCl_3$): δ = 140.06, 139.94, 139.77, 138.72, 137.21, 133.20, 132.98, 129.62, 127.32, 127.18, 125.68, 125.36, 124.78, 123.59, 122.88, 121.53, 121.02, 119.07, 111.91, 110.54, 109.16, 108.92 (Ar), 108.76, 108.25 (C≡C), 43.08, 31.21, 19.14, 13.53 (Bu), 15.11, 7.69 ppm (Et); ^{31}P{^{1}H} ($CDCl_3$): δ = 11.00 ppm ($^1J_{Pt,P}$ = 2629 Hz); FAB-MS: *m/z*: 1729 [M^+]; elemental analysis calcd (%) for $C_{88}H_{115}N_3P_4Pt_2$: C 61.13, H 6.70, N 2.43; found: C 61.01, H 6.56, N 2.50.

Synthesis of M3: A similar procedure to that for **M1** was employed by using **L3** (48 mg, 0.062 mmol) to produce a white solid in 22% yield (24 mg) after workup by TLC on silica by eluting with CH_2Cl_2/hexane (2:3, v/v). IR (CH_2Cl_2): $\tilde{\nu}$ = 2095 ν(C≡C) cm^{-1}; ^{1}H NMR ($CDCl_3$): δ = 8.32 (s, 2H, Ar), 8.09 (s, 2H, Ar), 7.82–7.69 (m, 8H, Ar), 7.53–7.24 (m, 8H, Ph + Ar), 6.96 (t, *J* = 13.5 Hz, 4H, Ph), 6.79 (t, *J* = 8.1 Hz, 4H, Ph), 4.30 (t, *J* = 8.1 Hz, 4H, CH_2), 2.08–2.03 (m, 4H, CH_2), 1.84–1.58 (m, 28H, CH_2 of Et + CH_2 of Bu), 1.58–1.24 (m, 4H, CH_2), 1.24–1.03 (m, 40H, CH_2 of Et + CH_2 of Bu), 0.99–0.92 (m, 6H, CH_3), 0.80–0.70 ppm (m, 10H, CH_2CH_3); ^{13}C NMR ($CDCl_3$): δ = 151.60, 140.97, 140.10, 139.27, 138.71, 132.63, 130.89, 128.80, 127.20, 126.09, 125.00, 123.27, 122.81, 122.40, 121.72, 121.06, 120.21, 119.74, 118.92, 110.53, 109.17, 108.76 (Ar), 108.32, 71.76 (C≡C), 55.12 (quat. C), 42.93, 40.35, 31.17, 26.06, 23.13, 20.54, 19.13, 13.35 (Bu), 15.26, 7.68 ppm (Et); ^{31}P{^{1}H} ($CDCl_3$): δ = 10.97 ppm ($^1J_{Pt,P}$ = 2629 Hz); FAB-MS: *m/z*: 1784 [M^+]; elemental analysis calcd (%) for $C_{93}H_{124}N_2P_4Pt_2$: C 62.61, H 7.01, N 1.57; found: C 62.55, H 7.12, N 1.46.

Acknowledgements

This research was supported by the Natural Sciences and Engineering Research Council of Canada, the Hong Kong Research Grants Council (CERG Grant: HKBU 202607) and the Hong Kong Baptist University (FRG/06–07/II-63).

[1] a) X. Xiao, Y. Fu, M. Sun, L. Li, Z. Bo, *J. Polym. Sci. A: Polym. Chem.* **2007**, *45*, 2410; b) W. Li, J. Qiao, L. Duan, L. Wang, Y. Qiu, *Tetrahedron* **2007**, *63*, 10161; c) H. Shao, X. Chen, Z. Wang, P. Lu, *J. Lumin.* **2007**, *127*, 349; d) R. Liu, Y. Xiong, W. Zeng, Z. Wu, B. Du, W. Yang, M. Sun, Y. Cao, *Macromol. Chem. Phys.* **2007**, *208*, 1503; e) M. C. Yuan, P. I. Shih, C. H. Chien, C. F. Shu, *J. Polym. Sci., Part A: Polym. Chem.* **2007**, *45*, 2925; f) H. Zhen, J. Luo, W. Yang, Q. Chen, L. Ying, J. Zou, H. Wu, Y. Cao, *J. Mater. Chem.* **2007**, *17*, 2824; g) A. Kruzinauskiene, A. Matoliukstyte, A. Michaleviciute, J. V. Grazulevicius, J. Musnickas, V. Gaidelis, V. Jankauskas, *Synth. Met.* **2007**, *157*, 401.

[2] a) J. H. Park, N. S. Cho, Y. K. Jung, H. J. Cho, H. K. Shim, H. Kim, Y. S. Lee, *Org. Electron.* **2007**, *8*, 272; b) K. Zhang, Z. Chen, Y. Zou, C. Yang, J. Qin, Y. Cao, *Organometallics* **2007**, *26*, 3699; c) R. Grisorio, P. Mastrorilli, C. F. Nobile, G. Romanazzi, G. P. Suranna, G. Gigli, C. Piliego, G. Ciccarella, P. Cosma, D. Acierno, E. Amendola, *Macromolecules* **2007**, *40*, 4865; d) Q. D. Liu, J. Lu, J. Ding, M. Day, Y. Tao, P. Barrios, J. Stupak, K. Chan, J. Li, Y. Chi, *Adv. Funct. Mater.* **2007**, *17*, 1028; e) M. Haeussler, J. Liu, R. Zheng, J. W. Y. Lam, A. Qin, B. Z. Tang, *Macromolecules* **2007**, *40*, 1914.

[3] a) Q. Peng, M. Li, S. Lu, X. Tang, *Macromol. Rapid Commun.* **2007**, *28*, 785; b) V. Promarak, M. Ichikawa, T. Sudyoadsuk, S. Saengsuwan, S. Jungsuttiwong, T. Keawin, *Synth. Met.* **2007**, *157*, 17; c) S. Bettington, M. Tavasli, M. R. Bryce, A. Beeby, H. Al-Attar, A. P. Monkman, *Chem. Eur. J.* **2007**, *13*, 1423; d) V. Promarak, A. Pankvuang, S. Ruchirawat, *Tetrahedron Lett.* **2007**, *48*, 1151; e) S. Grigalevicius, L. Ma, Z. Y. Xie, U. Scherf, *J. Polym. Sci., A: Polym. Chem.* **2006**, *44*, 5987.

[4] a) Z. Zhao, Y. Zhao, P. Lu, W. Tian, *J. Phys. Chem. C* **2007**, *111*, 6883; b) C. W. Wu, H. C. Lin, *Macromolecules* **2006**, *39*, 7232; c) M. Li, S. Tang, F. Shen, M. Liu, W. Xie, H. Xia, L. Liu, L. Tian, Z. Xie, P. Lu, M. Hanif, D. Lu, G. Cheng, Y. Ma, *J. Phys. Chem. B* **2006**, *110*, 17784; d) M. Li, S. Tang, F. Shen, M. Liu, W. Xie, H. Xia, L. Liu, L. Tian, Z. Xie, P. Lu, M. Hanif, D. Lu, G. Cheng, Y. Ma, *Chem. Commun.* **2006**, 3393; e) P. I. Shih, C. L. Chiang, A. K. Dixit, C. K. Chen, M. C. Yuan, R. Y. Lee, C. T. Chen, E. W. G. Diau, C. F. Shu, *Org. Lett.* **2006**, *8*, 2799; f) K. T. Wong, Y. M. Chen, Y. T. Lin, H. C. Su, C. C. Wu, *Org. Lett.* **2005**, *7*, 5361; g) C.-L. Ho, W.-Y. Wong, G.-J. Zhou, B. Yao, Z. Xie, L. Wang, *Adv. Funct. Mater.* **2007**, *17*, 2925.

[5] a) C. H. Liu, S. H. Chen, Y. Chen, *J. Polym. Sci., A: Polym. Chem.* **2006**, *44*, 3882; b) S. Lu, T. Liu, L. Ke, D. G. Ma, S. J. Chua, W. Huang, *Macromolecules* **2005**, *38*, 8494; c) C. W. Wu, C. M. Tsai, H. C. Lin, *Macromolecules* **2006**, *39*, 4298; d) X. M. Liu, J. Xu, X. Lu, C. He, *Macromolecules* **2006**, *39*, 1397; e) C. L. Liu, W. C. Chen, *Macromol. Chem. Phys.* **2005**, *206*, 2212; f) J. Du, Q. Fang, D. Bu, S. Ren, A. Cao, X. Chen, *Macromol. Rapid Commun.* **2005**, *26*, 1651.

[6] a) W. Y. Wong, *J. Inorg. Organomet. Polym. Mater.* **2005**, *15*, 197; b) W. Y. Wong, C. L. Ho, *Coord. Chem. Rev.* **2006**, *250*, 2627; c) C. E. Powell, M. G. Humphrey, *Coord. Chem. Rev.* **2004**, *248*, 725; d) A. S. Abd-El-Aziz, *Macromol. Rapid Commun.* **2002**, *23*, 995; e) N. J. Long, C. K. Williams, *Angew. Chem.* **2003**, *115*, 2690; *Angew. Chem. Int. Ed.* **2003**, *42*, 2586; f) I. Manners, *Science* **2001**, *294*, 1664; g) U. H. F. Bunz, *Chem. Rev.* **2000**, *100*, 1605; h) W.-Y. Wong, *Dalton Trans.* **2007**, 4495; i) W.-Y. Wong, *Macromol. Chem. Phys.* **2008**, *209*, 14.

[7] I. Manners, *Synthetic Metal-Containing Polymers*, Wiley-VCH, Weinheim, **2004**.

[8] N. Zhang, A. Hayer, A. Köhler, *J. Chem. Phys.* **2006**, *124*, 244701.

[9] J. Chen, J. Chen, S. Li, L. Zhang, G. Yang, Y. Li, *J. Phys. Chem. B* **2006**, *110*, 4663.

[10] D. Wasserberg, S. P. Dudek, S. C. J. Meskers, R. A. J. Jansen, *Chem. Phys. Lett.* **2005**, *411*, 273.

[11] a) B. Zelent, P. Messier, S. Gauthier, D. Gravel, G. Durocher, *J. Photochem. Photobiol. A* **1990**, *52*, 165; b) B. Zelent, P. Messier, D. Gravel, S. Gauthier, G. Durocher, *J. Photochem. Photobiol. A* **1987**, *40*, 145; c) T. Ganguly, D. K. Sharma, S. Gauthier, D. Gravel, G. Durocher, *J. Phys. Chem.* **1992**, *96*, 3757; d) K. Brummer, A. V. Dijken, H. Börner, J. J. A. M. Bastiaansen, M. M. Kiggen, B. M. W. Langeveld, *J. Am. Chem. Soc.* **2004**, *126*, 6035; e) Y. Cherkasov, E. L. Aleksandrova, Y. R. Piryatskii, *Opt. Spektros.* **1999**, *87*, 943.

[12] W. Y. Wong, W. K. Wong, P. R. Raithby, *J. Chem. Soc. Dalton Trans.* **1998**, 2761.

[13] M. S. Khan, M. R. A. Al-Mandhary, M. K. Al-Suti, B. Ahrens, M. F. Mahon, L. Male, P. R. Raithby, C. E. Boothby, A. Kohler, *Dalton Trans.* **2003**, 74.

[14] a) G. J. Zhou, W. Y. Wong, D. Cui, C. Ye, *Chem. Mater.* **2005**, *17*, 5209; b) M. S. Khan, M. R. A. Al-Mandhary, M. K. Al-Suti, B. Ahrens, M. F. Mahon, L. Male, P. R. Raithby, C. E. Boothby, A. Köhler, *Dalton Trans.* **2003**, 74; c) L. A. Emmert, W. Choi, J. A. Marshall, J. Yang, L. A. Meyer, J. A. Brozik, *J. Phys. Chem. A* **2003**, *107*, 11340.

[15] N. J. Turro, *Modern Molecular Photochemistry*, Benjamen/Cummings, London, **1978**.

[16] Presence of localized T_1 states and T_1 energy transfer in bis(ethynylchromophore)-containing oligomers were previously reported by Schanze et al., but their rates were not reported nor the S_1 quenching addressed. a) K. S. Schanze, E. E. Silverman, X. Zhao, *J. Phys. Chem. B* **2005**, *109*, 18451; b) E. E. Silverman, T. Cardolaccia, X. Zhao, K. Y. Kim, K. Haskins-Glusac, K. S. Schanze, *Coord. Chem. Rev.* **2005**, *249*, 1491.

[17] S. Faure, C. Stern, E. Espinosa, R. Guilard, P. D. Harvey, *Chem. Eur. J.* **2005**, *11*, 3469.

[18] P. Harvey, in *Porphyrin Handbook* (Eds.: K. M. Kadish, K. M. Smith, R. Guilard), Academic Press, Boston, **2003**, *18*, 63.

[19] J. V. Morris, M. A. Mahaney, J. R. Huber, *J. Phys. Chem.* **1976**, *80*, 969.

[20] O. Paliulis, J. Ostrauskaite, V. Gaidelis, V. Jankauskas, P. Strohriegl, *Macromol. Chem. Phys.* **2003**, *204*, 1706.

[21] W. Y. Wong, G. L. Lu, K. H. Choi, J. X. Shi, *Macromolecules* **2002**, *35*, 3506.
[22] J. Chatt, B. L. Shaw, *J. Chem. Soc.* **1960**, 4020.
[23] a) G. B. Kauffman, L. A. Teterm, *Inorg. Synth.* Vol. VII, **1963**, p. 245; b) J. Chatt, R. G. Hayter, *J. Chem. Soc. Dalton Trans.* **1961**, 896.
[24] A. D. Becke, *J. Chem. Phys.* **1993**, *98*, 5648.
[25] C. Lee, W. Yang, R. G. Parr, *Phys. Rev. B* **1988**, 785.
[26] B. Miehlich, A. Savin, H. Stoll, H. Preuss, *Chem. Phys. Lett.* **1989**, *157*, 200.
[27] K. D. Dobbs, W. J. Hehre, *J. Comput. Chem.* **1986**, *7*, 359.
[28] K. D. Dobbs, W. J. Hehre, *J. Comput. Chem.* **1987**, *8*, 861.
[29] a) M. Thelakkat, H.-W. Schmidt, *Adv. Mater.* **1998**, *10*, 219; b) R. S. Ashraf, M. Shahid, E. Klemm, M. Al-Ibrahim, S. Sensfuss, *Macromol. Rapid Commun.* **2006**, *27*, 1454.

Received: February 19, 2008
Published online: July 28, 2008

